J Atmos Chem (2009) 63:157–186
DOI 10.1007/s10874-010-9162-1

Automated mechanism generation. Part 2: application to atmospheric chemistry of alkanes and oxygenates

Shumaila S. Khan · Linda J. Broadbelt

Received: 30 November 2009 / Accepted: 17 June 2010 /
Published online: 13 July 2010

Abstract In this study, an automated mechanism generation framework was applied to atmospheric chemistry of volatile organic compounds (VOCs) and nitrogen oxides (NO_x). The framework generates reactions with minimal input based on a small set of reaction operators and includes a hierarchy for specifying rate constants for every reaction created. Mechanisms were generated for formaldehyde-air-NO_x, acetaldehyde-formaldehyde-*n*-octane-air-NO_x, and acetone-air-NO_x, and the model results were compared to experimental data obtained from smog chambers and to the SAPRC-99 lumped models. The models generated captured the experimental data very well, and their mechanistic formulation provided new insights into the controlling reaction pathways to pollutant formation. The approach applied here is sufficiently general that it can be applied to a wide range of alkane and oxygenate mixtures.

Keywords Mechanistic modeling · Ozone formation · VOC mixtures · Kinetic modeling

1 Introduction

Ozone is a major component of photochemical smog, an important air quality problem. Emission of volatile organic compounds (VOCs) into the atmosphere leads to increases in the ambient ozone concentration because nitrogen oxides (NO_x), primarily from vehicle exhaust, interact with VOCs in the presence of sunlight. While

Electronic supplementary material The online version of this article (doi:10.1007/s10874-010-9162-1) contains supplementary material, which is available to authorized users.

S. S. Khan · L. J. Broadbelt (✉)
Department of Chemical and Biological Engineering, Northwestern University,
Evanston, IL 60208-3120, USA
e-mail: broadbelt@northwestern.edu

it is known that different organics in the atmosphere vary in their reactivity and thus their contribution to ozone formation, it would be extremely valuable to have the ability to determine how significantly a particular VOC contributes to ozone formation (Bowman and Seinfeld 1994; Carter and Atkinson 1987, 1989).

VOC-NO_x chemistry of the atmosphere is complex, and many attempts have been made to determine the mechanism for reaction of various VOCs as well as study the kinetics for different types of hydrocarbons (Saunders et al. 2003; Aschmann et al. 2001; Atkinson 2000, 1997; Atkinson et al. 1995, 1997, 2000; Calvert et al. 2000; Carter and Atkinson 1996). Modeling has played an important role in these efforts, and indeed, many models have been proposed in the literature in recent years to account for ozone formation from VOCs in the presence of NO_x (Dodge 2000). Since atmospheric reaction mechanisms can get very large, even the most detailed mechanisms adopt some form of a priori mechanism reduction strategy. Most commonly, lumping strategies which either lump the species by their molecular classifications or their structure (i.e., bond types) are implemented. Several similarities exist between the various lumped mechanisms that have been developed. All of them consider the chemistry of inorganic species identically. These species are NO, NO_2, NO_3, N_2O_5, O_3, $O(^1D)$, $O(^3P)$, OH, HO_2, HONO, HNO_3, HNO_4, H_2O_2, and CO. Because of the large amount of uncertainty in the reactions and rate parameters of aromatic and biogenic VOCs, all of the mechanisms contain highly parameterized chemistry that has been optimized to fit smog chamber data. Finally, all of the mechanisms are revised periodically to correct deficiencies and update the experimental information, and hence, each mechanism has several versions.

A well-known lumped structure mechanism is the Carbon Bond (CB) mechanism which is also widely used in air quality simulation models (AQSMs) and has been developed since 1976 by researchers at Systems Applications International (Gery et al. 1989). In general, this mechanism lumps molecules based on the types of bonds that they contain. A second mechanism based on the lumped molecule approach that is well known is the SAPRC-99 mechanism developed at the Statewide Air Pollution Research Center by Carter and co-workers (Carter 2000). The SAPRC-99 mechanism contains more than three times the number of organic species as the CB mechanism, but lumping is still performed. As an illustration, reactions of alkanes with OH are represented in the mechanism by Eq. 1:

$$Alkane + OH \rightarrow aPROD_a + bPROD_b + cPROD_c + ... + nPROD_n \tag{1}$$

where a, b, c,..., n are the stoichiometric coefficients or product yield parameters of the products of the reaction. For this reaction type, there are rate constants available for many different types of alkanes. Therefore, depending on the system being modeled, the user specifies what species are to be lumped together, and these are referred to as the generalized species. For example, if the user wants to model a mixture of four alkanes, either one generalized species may be defined, or if the rates are different for each of the four species, two or more generalized species may be used. Parameters for the generalized reaction are then derived from the rate data. Once the product yield parameters and rate constants are defined, they are fixed throughout the simulation. Reactions of peroxy radicals are reduced by using a universal peroxy radical operator that counts the number of NO to NO_2 conversions for each peroxy radical that is formed. Several classes of peroxy radical operators are identified to represent acyl peroxy radicals and phenoxy radicals. The SAPRC-99 mechanism contains a total of 54 species and 158 reactions.

Other lumped molecule mechanisms are the Regional Acid Deposition Model (RADM) (Stockwell et al. 1990) and the Regional Atmospheric Chemistry Mechanism (RACM) (Stockwell et al. 1997), which is an update to the RADM. These are similar to the other lumped approaches, but they contain more explicit representations of the peroxy radical reactions. This expansion is limited to consideration of HO_2 and CH_3O_2 radicals, while larger radicals are ignored. The RADM and RACM mechanisms contain a total of 55 and 69 species, respectively, and 156 and 236 reactions, respectively.

Beyond lumped mechanisms, explicit mechanisms have also been proposed. Derwent et al. developed an explicit mechanism for 95 VOCs containing 515 chemical species and 900 reactions (Derwent et al. 1996). This was still not a comprehensive mechanism because it was condensed by treating peroxy radical chemistry in a simplified fashion and neglecting particular reaction intermediates. Jenkin et al. also developed an explicit mechanism for 120 VOCs containing 2,500 chemical species and approximately 7,000 reactions (Jenkin et al. 1997). This mechanism required ignoring minor reaction pathways and parameterization of peroxy radical reactions. This parameterization of peroxy radical reactions condensed the number of reactions involving peroxy species from 12,500 to 500. Makar et al. have also developed condensation schemes for explicit mechanisms which alter the differential equations for VOC reactants in order to limit the number of reactants by lumping them (Makar et al. 1996). One such scheme was used in a later study by these authors, but the reduced mechanism was almost as large as an explicit mechanism. This is because the reduction method could not be used to condense the reaction intermediates or products (Makar and Polavarapu 1997). Finally, a more recent approach used by Aumont et al. uses a similar approach to the one used in this paper (Aumont et al. 2005). The major differences between their approach and ours is how the rate constant estimation correlations are setup and our use of a rate-based generation algorithm.

In this study, automated mechanism generation was used to create models of the atmospheric chemistry of alkanes and oxygenates. The approach relies on definition of a small number of reaction operators that are applied repeatedly to different reactants. The framework also includes a hierarchy for specifying rate constants for every reaction generated. The methodology was applied to examine the reactivity of several different VOC single components and mixtures. Specifically, models were generated for formaldehyde-air-NO_x, acetaldehyde-formaldehyde-*n*-octane-air-NO_x, and acetone-air-NO_x, and the results were compared to experimental data. Furthermore, the model results were compared to the results of the SAPRC-99 model.

2 Methodology

2.1 Automated mechanism generation

Automated mechanism generation is a tool which generates reactions for the chemistry of interest based on a graph theoretic representation of species (Ranzi et al.

1995; Tomlin et al. 1992; Hillewaert et al. 1988; Matheu et al. 2001; Broadbelt et al. 1994a, b, 1995, 1996; Pfaendtner and Broadbelt 2008a, b; Wong et al. 2004a, b). Information is provided about the reactants and the reaction types, and the computer transforms this information into the reaction network, i.e., a list of reactant/product pairs. Computer generation of reaction species, properties and networks relies on a graph theory representation of molecules. The adjacency matrix for a graph, G, is the n-by-n matrix $M = (m_{ij})$ with elements 0 and 1, such that $m_{ij} = 1$ if (v_i, v_j) is an edge of G or a connection between vertices (or atoms) of G and $m_{ij} = 0$ otherwise (Tarjan 1977). The bond and electron (BE) matrix augments the adjacency matrix and provides a description of not only the connectivity of a molecule but also its formal electronic state (Ugi et al. 1979). The diagonal element, *ii*, of the BE matrix gives the number of non-bonded valence electrons of atom *i*, and off-diagonal entries, *ij*, provide the connectivity and bond order of atoms *i* and *j*. An example BE matrix for ethyl radical is shown in Fig. 1. The rows of the BE matrix correspond to the atoms in the order in which they are numbered in the picture on the left.

Chemical reaction may then be carried out via simple manipulations of the BE matrices of reactant molecules. The BE matrix is well suited for description of chemical reactions because the number of atoms actually affected in a chemical reaction is small. The BE sub-matrix comprising only those atoms is small and dense. To carry out a particular reaction type, the reaction matrix that quantifies the change in the electronic configurations and the connectivity among the atoms affected by reaction is determined. The reaction matrices can be identified by simple matrix subtraction operations of the reactant and product matrices. This is illustrated in Fig. 2 for a hydrogen abstraction reaction. First, the reactants, methane and hydrogen radical, and products, methyl radical and hydrogen, are represented by their BE matrices. The two matrices for the reactants are combined into one matrix, and the same is done for the products. The matrices are then permuted in a consistent manner so that the atoms that will experience the bond breaking, bond formation, or change in number of non-bonded electrons are moved to the upper left hand corner. The reaction matrix for hydrogen abstraction is then calculated by the difference between the reactant and product matrices. The reaction matrix thus obtained is general and can now be applied to any combination of a radical and a substrate with an abstractable hydrogen. To apply automatic mechanism generation to a new chemistry, it is necessary to determine the reaction matrices for the reaction types involved. For atmospheric chemistry, operators were formulated for the reaction types discussed in detail in part 1 of this paper. For the alkanes and oxygenates investigated here, all reaction types in Table 1 were applied.

Fig. 1 Molecular structure of ethyl radical and its bond-electron matrix representation that specifies atomic connectivity

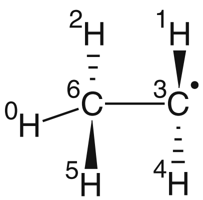

$$\begin{array}{c} H^0 \\ H^1 \\ H^2 \\ C\bullet^3 \\ H^4 \\ H^5 \\ C^6 \end{array}\begin{bmatrix} 0 & 0 & 0 & 0 & 0 & 0 & 1 \\ 0 & 0 & 0 & 1 & 0 & 0 & 0 \\ 0 & 0 & 0 & 0 & 0 & 0 & 1 \\ 0 & 1 & 0 & 1 & 1 & 0 & 1 \\ 0 & 0 & 0 & 1 & 0 & 0 & 0 \\ 0 & 0 & 0 & 0 & 0 & 0 & 1 \\ 1 & 0 & 1 & 1 & 0 & 1 & 0 \end{bmatrix}$$

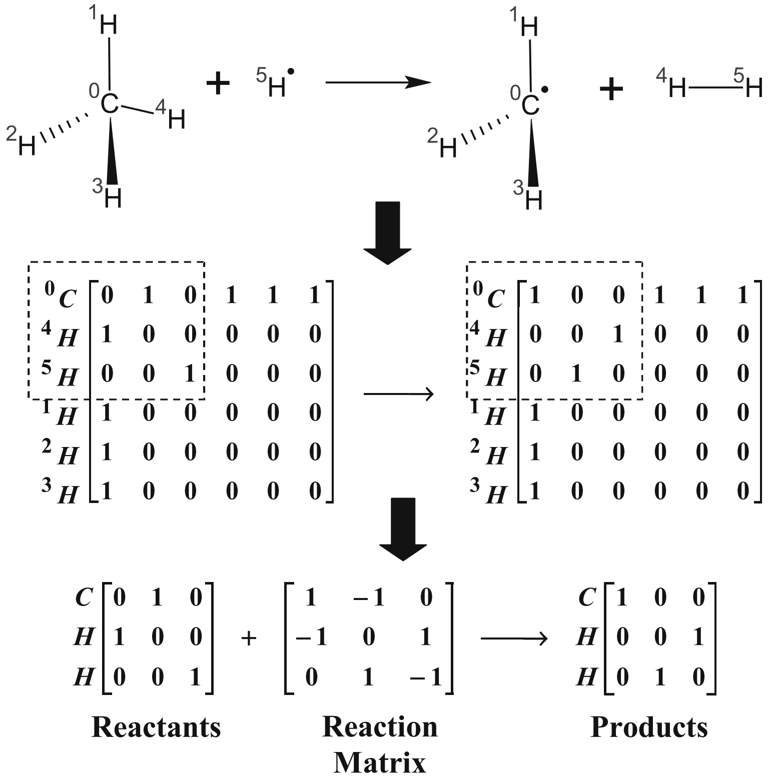

Fig. 2 Development of a reaction matrix for a hydrogen abstraction reaction. Atoms in reactants and products are numbered and converted into BE matrices. The submatrices are combined, and the atoms that are affected in the reaction are moved to the *top*. The matrices for the affected atoms are extracted, and a reaction matrix is found by subtracting the reactant submatrix from the product submatrix

The basic algorithm for generating reaction mechanisms is to repeatedly apply the set of reaction matrices to the reactants and their progeny that have the necessary functionality to undergo each reaction. However, it is possible to generate an infinite set of reactions. To control growth of the mechanisms generated, the rate-based termination approach developed by Susnow et al. was applied (Susnow et al. 1997). The rate-based generation criterion aims to include an important species in the mechanism as it is generated based on its rate of formation (Susnow et al. 1997; De Witt 1999; DeWitt et al. 2000). The reactants and model conditions (i.e., temperature, pressure, reactor type, reaction time) are specified that are representative of the experimental conditions to which the model will be applied. Initially, the reactant species are specified and form the initial *reactive* species pool. The reaction time is divided into intervals, with smaller intervals at earlier times. The reactions for the *reactive* species are carried out, and the unique species that are formed are the *unreactive* species that will only be allowed to react if they meet certain criteria. Once the reactions are generated, the model is solved for the time interval that is currently

Table 1 Kinetic correlations for all thermal reaction families

Reaction family	E_o	A_{for}	α_{for}	A_{rev}	α_{rev}	Reverse reaction family	Note(s)
Hydrogen abstraction	13.3	1.66×10^{-10}	0.3	1.66×10^{-10}	0.7	Hydrogen abstraction	H radical[a]
	13.3	1.66×10^{-13}	0.3	1.66×10^{-13}	0.7		C radical[a]
	7.02	9.20×10^{-13}	–	–	–		(HR)– O radical[b,c]
	8.31	2.03×10^{-12}	–	–	–		NO_3 radical[b,c]
Bond fission	0	1.0×10^{16}	1.0	1.66×10^{-12}	0	Radical recombination	C–C, C–O, O–O
	0	1.67×10^{16}	1.0	6.47×10^{-12}	0		N–N, N–O
Oxygen addition	4.25	1.57×10^{-11}	0.11	3.47×10^{15}	0.89	β-scission	
Rev. peroxy & NO radical recombination	0	2.75×10^{15}	1	1.66×10^{-12}	0	Peroxy & NO radical recombination	
Rev. peroxy & NO radical reaction	0	1.15×10^{-11}	1	1.15×10^{-11}	0	Peroxy & NO radical reaction	
Oxygen disproportionation	Structure-based			–	–	–[d,e]	
Peroxy radical disproportionation	Structure-based			–	–	–[d,e]	
Rev. peroxy radical recombination	0	3.40×10^{-11}	1	6.81×10^{-12}	0	Peroxy radical recombination	$HO_2 + RO_2$
	0	1.43×10^{-13}	1	2.71×10^{-15}	0		$RO_2 + RO_2$
Peroxy & HO_2 radical reaction	1.30×10^{-13} exp(1.84/RT)			–	–	–[e]	
Rev. alkoxy radical & NO_x reaction	0	5.37×10^{-12}	1	4.78×10^{-12}	0	Alkoxy radical & NO_x reaction	NO radical
	0	1.21×10^{-12}	1	1.67×10^{-12}	0		NO_2 radical
Alkoxy radical & oxygen reaction	6.56	2.70×10^{-14}	0.17	–	–	–[e]	

β-scission	14.24	1.00×10^{14}	0.76	1.66×10^{-13}	0.24	Radical addition	C radical
	10.0	1.21×10^{13}	0.47	–	–		RO radical[c,f]
	6.10	2.27×10^{11}	0.96	–	–		RO radical[c,g]
One-five radical shift	12	2.00×10^{10}	0.50	2.00×10^{10}	0.50	One-five radical shift	H to C radical
	9.35	1.04×10^{12}	0.50	3.81×10^{10}	0.50		H to O radical
Carbon radical & oxygen reaction	14.45	1.90×10^{-11}	0.70	–	–	–[e]	
Radical addition	7.44	2.83×10^{-11}	0.24	–	–	β-scission	(HR)–O radical[c]
	21.23	2.91×10^{-12}	1	–	–		NO_3 radical[c]

Units for rate constants are cm^3 $molecule^{-1}$ s^{-1} or s^{-1} and intrinsic activation energy barrier are kcal mol^{-1}

[a] Since both forward and reverse reaction families are hydrogen abstraction the forward reaction is set to be the endothermic reaction

[b] Blowers and Masel correlation (Blowers and Masel 1999)

[c] Reverse reaction rate constant is calculated based on equilibrium relations

[d] Activation energy from an empirical expression based on the number of carbons and degree of substitution on the peroxy radical; cross-reaction rate constants are two times the geometric mean of the self-reaction rate constants. Use estimate of rate constant from Kirchner and Stockwell (1996) and use branching ratios of Madronich and Calvert (1990)

[e] Reverse reaction family not implemented in mechanism generation algorithm

[f] Heat of reaction >5 kcal mol^{-1}

[g] Heat of reaction $\leq$5 kcal mol^{-1}

being analyzed. A characteristic rate of change for the system, R_{char}, is calculated as shown in Eq. 2:

$$R_{char} = max(|r_i|) \tag{2}$$

where r_i is the net rate of formation of species i, and the maximum from the set of all *reactive* species' r_i values is selected as R_{char}. A minimum rate of formation, R_{min}, for a species to be considered *reactive* is then calculated based on Eq. 3 using the R_{char} value from Eq. 2:

$$R_{min} = \varepsilon R_{char} \tag{3}$$

where ε is a user-defined threshold which must be greater than zero. The species with the largest rate of formation, $r_{j,max}$, is then selected from the *unreactive* species list. If $r_{j,max}$ is greater than R_{min}, species j is added to the *reactive* species pool; otherwise, this test is performed for the next time subinterval until the final simulation time is reached and no more reactions or species are included. However, if a species is added to the *reactive* species pool, the reactions which this species undergoes must also be generated, and the process is repeated for determining the characteristic rate and including additional reactions. For lower threshold values (ε), larger mechanisms are generated, and thus, the mechanism size can be tailored by selecting ε.

2.2 Air-NO_x chemistry

To ensure that all necessary reactions of small molecules in an air-NO_x mixture were included in every model generated regardless of the value of ϵ applied, all mechanisms were seeded with small molecules whose reactions are listed in part 1 of this paper and reproduced here in Table 2 along with their rate coefficients. Subsequent mechanism generation runs of different VOC-NO_x mixtures simply included all the air-NO_x reactions directly from a lookup table consisting of these reactions.

2.3 Mechanism convergence as a function of ϵ

Application of the rate-based criterion involved starting with an ϵ value equal to 1.0 and then lowering it, typically by factors of 10. To determine which mechanisms were likely to be sufficiently comprehensive, three criteria were used. First, important secondary products had to be included. The mechanisms were simply inspected for the presence of products reported experimentally. Second, a mechanism for a given value of ϵ was solved, and the concentrations of the major products (O_3, NO_2, NO, VOC, peroxy-acetyl nitrate) were calculated for a fixed set of kinetic parameters and using a batch reactor model. The threshold was then lowered by a factor of 10 in most cases, and new values of the concentrations were calculated and compared to the previous model results according to the maximum deviation (MD) defined in Eq. 4:

$$MD = 100 * max\left(\frac{\sum |C_{i,model\,1} - C_{i,model\,2}|}{\sum |C_{i,model\,1}|}\right) \tag{4}$$

where $C_{i,model\,1}$ and $C_{i,model\,2}$ are the concentrations of species i from *model* 1 and *model* 2. If the value of MD was less than 5%, then the mechanism was deemed sufficiently comprehensive. This threshold of 5% was selected based on extensive generation of the mechanism for formaldehyde-air-NO_x where ϵ was lowered until there was no change in the concentration values. Finally, the mechanisms were compared to experimental data and the kinetic parameters were required to lie within any specified uncertainty ranges.

2.4 Experimental data modeled

Experiments conducted at the Statewide Air Pollution Research Center (SAPRC) at the University of California at Riverside (Carter 2000; Carter et al. 1993, 1995; Carter and Lurmann 1991; Carter and Atkinson 1987) and at the University of North Carolina (UNC) (Jeffries et al. 1985) were used to evaluate the model results. To measure the overall ability of the model to capture the experimental data, a sum of squares error (SSE) was defined as in Eq. 5:

$$SSE = \sum_i \sum_j (C_{i,exp}(t_j) - C_{i,model}(t_j))^2 \quad (5)$$

where i represents a species with experimental data, j is a given time at which a measurement was taken, and C is concentration.

Experimental data collected in five different chambers were used. The experiments conducted at SAPRC were carried out in various collapsible smog chambers containing different light sources and of variable size. Three of the chambers employed a blacklight source and consisted of a Teflon bag in which the reactants were injected and irradiated: the evacuable (~3,000 L), dividable (2 ~5,000 L chambers), and indoor (~6,400 L) chambers are denoted as ETC, DTC, and ITC, respectively. The fourth distinct chamber used a xenon arc light source and consisted of a Teflon chamber (~5,000 L) denoted by XTC. All the SAPRC experiments modeled in this work include the radical source reactions that have been characterized in the studies (Carter 2000). However, the effect of these reactions on the model results is minimal. The fifth chamber was an outdoor chamber (~300,000 L) at UNC that uses natural sunlight and is simply denoted by UNC.

It is important to note that while experimental measurements for the majority of the species were taken directly, measurement of NO_2 was done by passing the effluent through a NO_x converter. Since this will convert not only NO_2, but also alkyl nitrates and in some cases nitric acid, NO_2 measurements from the SAPRC smog chambers include all nitrates. Therefore, the composite concentration of all of these types of species was compared to the experimentally reported NO_2 concentration, which is henceforth referred to as nitrates.

The specific systems examined were formaldehyde-air-NO_x, formaldehyde-acetaldehyde-*n*-octane-air-NO_x, and acetone-air-NO_x. All mechanisms and results are discussed in the following sections.

2.5 Thermal rate constant estimation

The thermal rate constants that need to be estimated for the purposes of modeling atmospheric chemistry have been outlined in detail in part 1 of this paper. Therefore, the reader is directed to part 1 to become familiar with how these properties are determined. A summary of the kinetic parameters that are used for each reaction

Table 2 Air-NO_x chemistry included in all models

Thermal reactions					
Reaction	k	A	E_a	n[a]	Reference
$O_3 + NO \rightarrow O_2 + NO_2$	1.73×10^{-14}	1.40×10^{-12}	2.60		Atkinson et al. (2004)
$O_3 + NO_2 \rightarrow O_2 + NO_3$	3.52×10^{-17}	1.40×10^{-13}	4.91		Atkinson et al. (2004)
$O_3 + HO \rightarrow O_2 + HO_2$	7.25×10^{-14}	1.70×10^{-12}	1.87		Atkinson et al. (2004)
$O_3 + HO_2 \rightarrow O_2 + O_2 + HO$	2.01×10^{-15}	1.97×10^{-16}	−1.38	4.57	Atkinson et al. (2004)
$NO + NO + O_2 \rightarrow NO_2 + NO_2$	1.95×10^{-38}	3.30×10^{-39}	−1.05		Atkinson et al. (2004)
$NO + NO_3 \rightarrow NO_2 + NO_2$	2.60×10^{-11}	1.80×10^{-11}	−0.22		Atkinson et al. (2004)
$NO_2 + NO_3 \rightarrow NO + NO_2 + O_2$	6.56×10^{-16}	4.50×10^{-14}	2.50		DeMore et al. (1997)
$NO_3 + NO_3 \rightarrow NO_2 + NO_2 + O_2$	2.29×10^{-16}	8.50×10^{-13}	4.87		DeMore et al. (1997)
$NO_3 + HO \rightarrow HO_2 + NO_2$	2.00×10^{-11}				Atkinson et al. (2004)
$NO_3 + HO_2 \rightarrow HO + NO_2 + O_2$	2.51×10^{-12}				Becker et al. (1992)
$NO_3 + HO_2 \rightarrow O_2 + HONO_2$	8.00×10^{-13}				Carter (2000)
$HO + HO \rightarrow H_2O + O(^3P)$	1.48×10^{-12}	6.20×10^{-14}	−1.88	2.6	Atkinson et al. (2004)
$HO + HO_2 \rightarrow H_2O + O_2$	1.11×10^{-10}	4.80×10^{-11}	−0.50		Atkinson et al. (2004)
$HO + CO \rightarrow H + CO_2$	2.09×10^{-13}				Carter (2000)
$HO_2 + HO_2 \rightarrow O_2 + H_2O_2$	1.80×10^{-12}	1.90×10^{-13}	−1.33		Kanno et al. (2006)
$HO_2 + H \rightarrow H_2 + O_2$	5.60×10^{-12}				Atkinson et al. (2004)
$HO_2 + H \rightarrow HO + HO$	7.20×10^{-11}				Atkinson et al. (2004)
$HO_2 + H \rightarrow H_2O + O(^3P)$	2.40×10^{-12}				Atkinson et al. (2004)
$N_2O_5 + H_2O \rightarrow HONO_2 + HONO_2$	2.50×10^{-22}				Atkinson et al. (2004)
$O(^3P) + O_2 + M \rightarrow O_3 + M$	5.70×10^{-34}	5.70×10^{-34}		−2.6	Atkinson et al. (2004)

$O(^3P) + O_3 \rightarrow O_2 + O_2$	7.96×10^{-15}	8.00×10^{-12}	4.09		Atkinson et al. (2004)
$O(^3P) + NO \rightarrow NO_2$	2.99×10^{-11}	2.99×10^{-11}		0.3	Atkinson et al. (2004)
$O(^3P) + NO_2 \rightarrow O_2 + NO$	1.03×10^{-11}	5.50×10^{-12}	−0.37		Atkinson et al. (2004)
$O(^3P) + NO_2 \rightarrow NO_3$	2.30×10^{-11}	2.30×10^{-11}		0.24	Atkinson et al. (2004)
$O(^3P) + NO_3 \rightarrow O_2 + NO_2$	1.70×10^{-11}				Atkinson et al. (2004)
$O(^3P) + HO \rightarrow O_2 + H$	3.47×10^{-11}	2.40×10^{-11}	−0.22		Atkinson et al. (2004)
$O(^3P) + HO_2 \rightarrow O_2 + HO$	5.73×10^{-11}	2.70×10^{-11}	−0.45		Atkinson et al. (2004)
$O(^1D) + N_2 \rightarrow O(^3P) + N_2$	2.58×10^{-11}	1.80×10^{-11}	−0.21		Atkinson et al. (2004)
$O(^1D) + O_2 \rightarrow O(^3P) + O_2$	4.01×10^{-11}	3.20×10^{-11}	−0.13		Atkinson et al. (2004)
$O(^1D) + H_2O \rightarrow HO + HO$	2.01×10^{-10}	1.62×10^{-10}	−0.13		Dunlea and Ravishankara (2004)
$HC\dot{O} + O_2 \rightarrow HO_2 + CO$	5.20×10^{-12}				Atkinson et al. (2001)
[b]$HO + NO_2 + M \rightarrow HONO_2 + M$	k_o	2.50×10^{-30}		−4.4	DeMore et al. (1997)
	k_∞	1.60×10^{-11}		−1.7	DeMore et al. (1997)

Photolysis reactions	
$NO_2 + hv \rightarrow NO + O(^3P)$	Used σ and ϕ data from DeMore et al. (1997)
$O_3 + hv \rightarrow O_2 + O(^1D)$	Used σ data from Molina and Molina (1986) and ϕ data from Talukdar et al. (1998)
$NO_3 + hv \rightarrow NO + O_2$	Used σ data from DeMore et al. (1997) and ϕ data from Johnston et al. (1996)

Rate constants are at 298 K. Units for rate constants and pre-exponential factors are either cm^3 $molecule^{-1}$ s^{-1} or cm^6 $molecule^{-2}$ s^{-1} and units for activation energy are kcal mol^{-1}

[a]$k = A\,(T/298)^n \exp(-E_a/RT)$

[b]Rate constant based on the Lindenmann-Hinshelwood expression as follows: $k(Z) = k(M,T) = \left(\frac{k_o(T)[M]}{1+(k_o(T)[M]/k_\infty(T))}\right) 0.6^{\{1+[log_{10}(k_o(T)[M]/k_\infty(T))]^2\}^{-1}}$

family is listed in Table 1 where the Arrhenius form for the rate coefficient is assumed. In most cases, the Evans–Polanyi relationship is utilized to estimate the Arrhenius activation energy, where the activation energy is related to the enthalpy of the reaction as represented by Eq. 6:

$$E_i = E_o + \alpha \Delta H_{rxn,i} \tag{6}$$

where E_o and α are constants obtained by fitting to experimental data. For the pre-exponential factor, it is often assumed that a single value is valid for all reactions in the family since the grouped reactions are entropically similar (Evans and Polanyi 1938). A variation of the Marcus equation is used to represent the hydrogen abstraction reactions (Blowers and Masel 1999). Structural relationships are used as well to represent some of the peroxy-peroxy radical reactions using work done by Kirchner and Stockwell (1996) and Madronich and Calvert (1990).

2.6 Photolysis rate constant estimation

It was necessary to estimate photochemical rate constants for reactions that are attributed to exposure to sunlight. As detailed in our previous work (Khan and Broadbelt 2004), photolysis rate constants depend on other factors besides the temperature and do not follow the Arrhenius form. Instead, the relationship presented in Eq. 7 is valid:

$$k_{photolysis} = \int_{\lambda} F(\lambda, \theta)\phi(\lambda, T)\sigma(\lambda, T)d\lambda \tag{7}$$

where F is the actinic flux, ϕ is the quantum yield, and σ is the absorption cross section (Finlayson-Pitts and Pitts 1999). Actinic flux is a function of the wavelength (λ) and solar zenith angle (θ) and is therefore not specific to any molecules. Rather it is a function of time of day and geography, or if indoor experiments are conducted, it is a function of the spectrum and intensity of the artificial light source. On the other hand, quantum yield and absorption cross section are mainly functions of wavelength, with only a weak dependence on temperature. Therefore, to estimate rate constants, it was necessary to specify the quantum yield and absorption cross section of a given molecule as a function of λ. The approach used to specify ϕ and σ is discussed in our previous work (Khan and Broadbelt 2004).

Methods were developed for calculation of photolysis rate constants in both outdoor and indoor environments. The factors that vary in these two environments are the spectra and intensity of the light source. For indoor chambers that were modeled, both blacklight and xenon arc light sources were used. For the outdoor chamber modeled, the light source is sunlight. For both indoor and outdoor chambers, all photolysis rate constants are referenced to the photolysis rate constant of NO_2 (k_{NO_2}) because only the relative intensity of the light source is typically known. The nitrate photolysis rate constants have been shown to have errors of up to 0.05 min^{-1} for some chambers using blacklight sources and ± 0.01 min^{-1} for the xenon arc light chamber.

For the indoor chamber experiments of Carter (2000), k_{NO_2} was calculated for a given characterization run by flowing NO_2 through a plug-flow reactor and measuring the amount of NO that was formed. These light characterization runs were carried out between actual VOC-NO_x runs. The values of k_{NO_2} for these runs were fit as a function of the run number, and depending on the experimental run number, k_{NO_2} for the particular VOC-NO_x run being modeled was predicted. The values for the photolysis rate constant for all other species for a particular run were then calculated from k_{NO_2} according to Eq. 8:

$$k_i = k_{NO_2} \frac{\int_\lambda J(\lambda)\phi_i(\lambda)\sigma_i(\lambda)d\lambda}{\int_\lambda J(\lambda)\phi_{NO_2}(\lambda)\sigma_{NO_2}(\lambda)d\lambda} \quad (8)$$

where $J(\lambda)$ is the spectrum for the particular light source and the rest of the properties are defined as in Eq. 7. For the xenon arc light source, runs had a measured spectrum for each run, and the blacklight source had a single measured spectrum that was not expected to change from run to run.

The approach used to estimate photolysis rate coefficients for outdoor experiments was slightly different because natural sunlight was used. The only information provided in the experimental data (Jeffries et al. 1985) was k_{NO_2} inside the chamber as a function of time, but the measured spectrum of sunlight was not available. Instead the solar zenith angle as a function of time was estimated based on the known solar zenith angles of 90°, 0°, and 90° for the sunrise, solar noon, and sunset times, respectively, reported for a given experiment. Given the estimated solar zenith angle as a function of time, $\theta_{est}(t)$, the value of $F(\lambda, \theta)$ could be specified by using a known sunlight spectrum at the Earth's surface and for clear conditions (best estimate of surface reflection and no light scattering or cloud cover) (Finlayson-Pitts and Pitts 1999). The predicted value of k_{NO_2} given $\theta_{est}(t)$ was then calculated using Eq. 7 with absorption cross-section data from Finlayson-Pitts and Pitts (1999) and ratioed to the known $k_{NO_2}(t)$ value measured experimentally. Photolysis rate coefficients for other species were then estimated according to Eq. 9:

$$k_i = k_{NO_2}(t) \frac{k_i(\theta_{est}(t))}{k_{NO_2}(\theta_{est}(t))} \quad (9)$$

where θ_{est} is the estimated solar zenith angle, t is the time, and k_i is the rate constant for photolysis of species i. The use of the ratio $k_{NO_2}(t)/k_{NO_2}(\theta_{est}(t))$ aimed to correct for any errors introduced by $F(\lambda, \theta)$.

3 Results

3.1 Formaldehyde-air-NO_x

A mechanism for formaldehyde-air-NO_x was developed using the rate-based mechanism generation strategy. The experiment used to generate this mechanism and to which a smog chamber model was compared was the SAPRC ETC smog chamber run number 441 (ETC-441) of Carter and coworkers (Carter et al. 1993). The initial concentrations of NO, NO_2, formaldehyde, and CO were 0.226, 0.048, 0.441, and 0.800 ppm, respectively. The temperature varied linearly from 300.5 to 301.0 K throughout the experiment, and the photolysis rate constant of NO_2 was reported as 0.351 min^{-1}. The threshold value, ϵ, was reduced by increments of an order of magnitude from 1 to 1×10^{-7}. Table 3 shows how the mechanism increased in size as the threshold value was decreased. More specifically, the table shows how the number of reactive species, thermal and photolysis reactions, SSE and MD varied as the threshold value was decreased. The number of species and thermal reactions consistently increased with threshold value while the number of photolysis reactions was fairly constant throughout. The mechanisms generated at the threshold values of 1.0 and 0.1 were identical. The SSE also converged to a constant value as the threshold was reduced. The convergence of the mechanism was also manifested in the value of MD, which dropped to 0.00% when ϵ was equal to 0.000001. Therefore, the mechanism at ϵ equal to 0.01 was chosen as the mechanism that contained all of the significant reactions since it was smaller then the 0.001 mechanism with nearly the same results.

The SSE values reported in Table 3 were all obtained based on experimental rate constants when available and estimation of unknown rate coefficients using the default parameters summarized in part 1 of this paper and in Table 1. When the concentrations of all primary products were compared to experimental data using these default parameters, it was found that the model results agreed well with experiment. The model results that are thus a pure prediction, i.e., no parameter fitting was performed, are shown in Fig. 3. Figure 4 shows the detailed mechanism for formaldehyde oxidation. The mechanism was analyzed, and net rates of all reactions were studied at 2, 4 and 6 h. Any net rate that was found to be above 6.023×10^6 molecule cm^{-3} s^{-1} at any of those times is shown in Fig. 4. Furthermore, reactions that utilize a kinetic correlation are identified in the mechanism.

In order to test the predictive capabilities of the model, the mechanism was used without any adjustment to model additional formaldehyde-air-NO_x runs at different conditions and in different smog chambers. First, the model predictions were compared to the UNC formaldehyde chamber experiment from July 15, 1988. The results for the concentrations of the major species are shown in Fig. 5. The model does quite a reasonable job in capturing the experimental data for this outdoor chamber. The mechanism was then tested on two other experiments in indoor chambers at different VOC/NO_x concentration ratios. In this case, VOC simply refers to formaldehyde. One of the experiments was conducted in the ETC chamber and was run number 378 (ETC-378), and the other was the SAPRC ITC chamber with run number 1554 (ITC-1554). The VOC/NO_x ratios for the ETC-378, ETC-441, and ITC-1554 experiments were 0.90, 1.61, and 2.32, respectively. Note that although the mechanism was generated using a specific initial VOC/NO_x ratio (1.61)

Table 3 Formaldehyde-air-NO_x model as a function of mechanism generation threshold value

ε	Species	Reactions		SSE[a]	MD
		Thermal	Photolysis		
1.0	25	81	13	2.76×10^{25}	
0.1	25	81	13	2.76×10^{25}	0.00
0.01	27	93	13	3.50×10^{25}	9.78
0.001	28	107	13	3.51×10^{25}	0.38
0.0001	32	123	15	3.50×10^{25}	0.11
0.00001	36	156	18	3.50×10^{25}	0.01
0.000001	39	191	18	3.50×10^{25}	0.00
0.0000001	48	235	18	3.50×10^{25}	0.00

[a]SSE = sum of squares error for NO, nitrates, O_3, and formaldehyde and has units of molecule^2 cm^{-6}

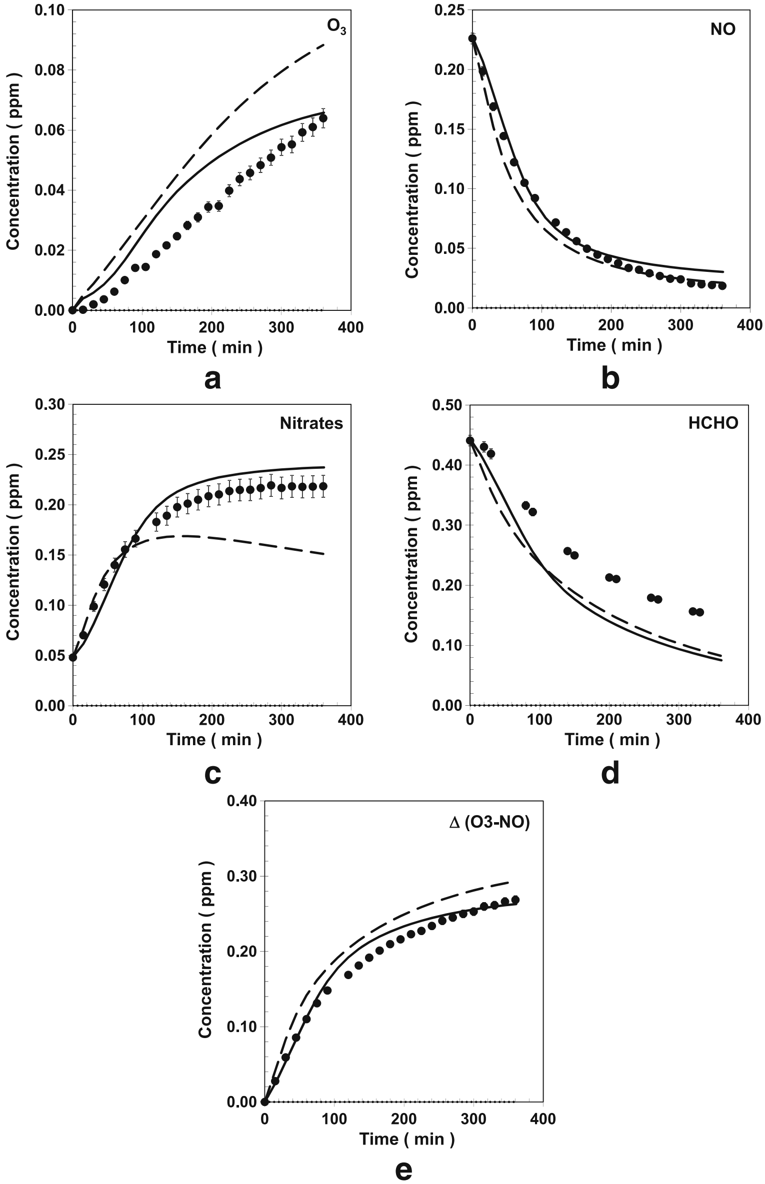

Fig. 3 Results of the formaldehyde-air-NO_x model compared to experimental data. The concentration versus time curves for ozone, NO, nitrates, formaldehyde, and $\Delta(O_3 - NO)$ correspond to **a**–**e**, respectively. Experimental data which is shown as the *symbols* were obtained from the SAPRC ETC smog chamber (ETC-441). The *solid lines* represent results from our models and *dashed lines* represent results from the SAPRC-99 model

to guide the rate-based generation, the final mechanism generated was not sensitive to the initial formaldehyde/NO_x ratio used. Various measures have been proposed as the best representation of the reactivity of VOCs (Carter 1994). One measure of

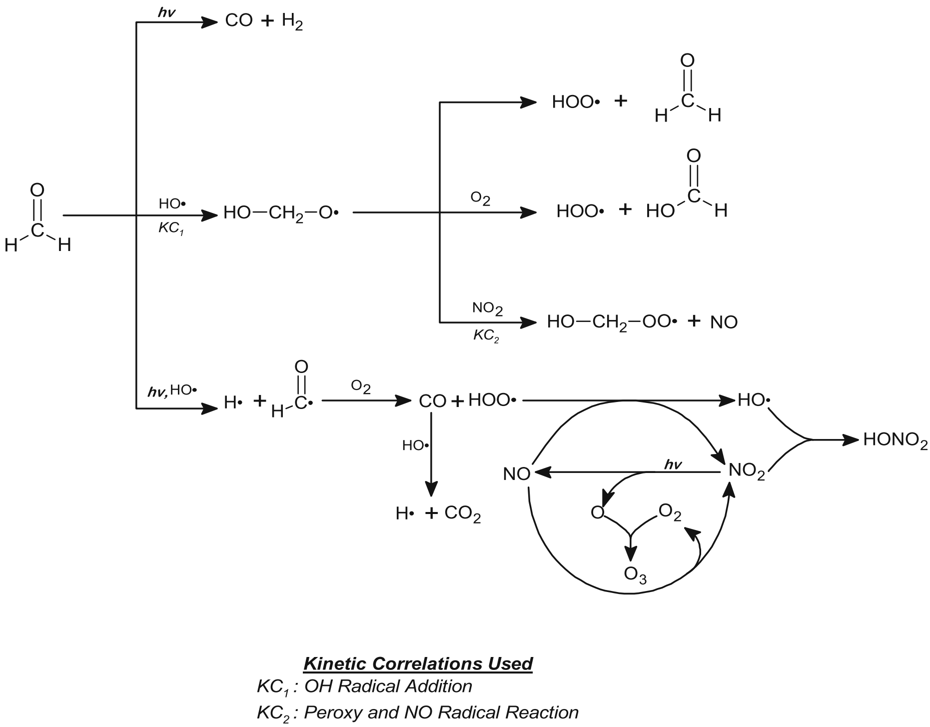

Fig. 4 The major reactions in the formaldehyde reaction mechanism. Small molecule reactions are not shown on the diagram and can be found in Table 2 and the Supplementary Information

how well the experimentally measured reactivity is represented by the model is to estimate the difference in the ozone and NO concentrations according to Eq. 10:

$$\Delta(O_3 - NO)(t) = (C_{O_3}(t) - C_{NO}(t)) - (C_{O_3}(t_i) - C_{NO}(t_i)) \tag{10}$$

where $C_{O_3}(t_i)$ and $C_{NO}(t_i)$ are the concentrations of ozone and NO initially. Figure 3 demonstrates how the formaldehyde model captures this reactivity measure for ETC-441 as a function of time, and the error compared to the experimental data is consistently lower than that observed for the SAPRC-99 model except for the VOC/NO_x ratio of 2.32. Figure 6 shows how the percent error of the $\Delta(O_3 - NO)$ values compares to experiment at selected reaction times. The errors from the SAPRC-99 model compared to experiment are also shown. The percent error of our model is quite low, especially for the two lowest VOC/NO_x ratios, and is consistently lower than the error observed for the SAPRC-99 model.

3.2 Acetaldehyde-formaldehyde-*n*-octane-NO_x

With the relatively compact formaldehyde-air-NO_x model in hand, the automated mechanism generation framework was applied to create a mechanism for a multi-component mixture of acetaldehyde, formaldehyde, *n*-octane, and NO_x. Experimental data for this system was available from SAPRC in the XTC chamber. Specifically,

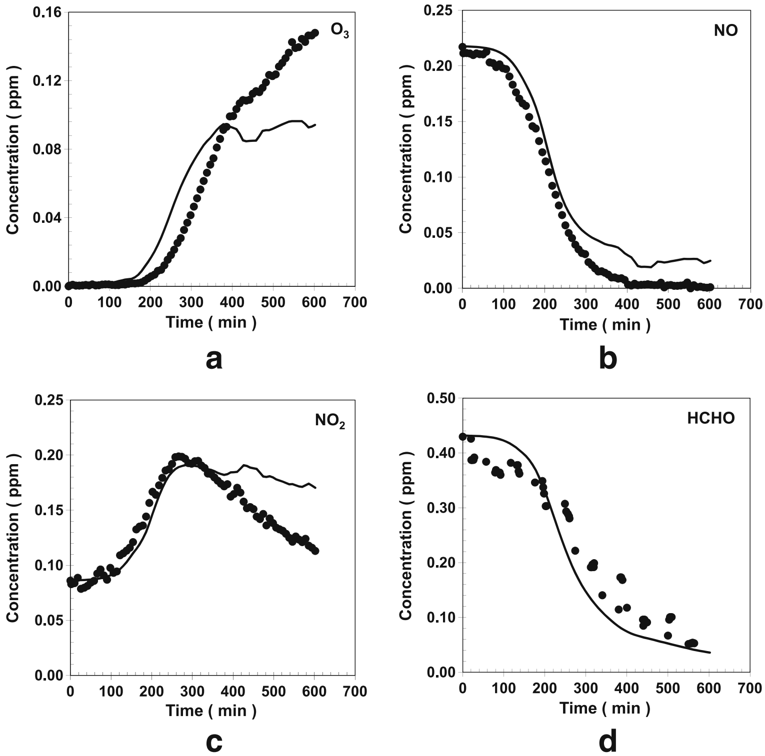

Fig. 5 The model predictions for the UNC chamber formaldehyde run from July 15, 1988. The concentration versus time curves for ozone, NO, NO_2, and formaldehyde correspond to **a**–**d**, respectively. Experimental data are represented by the *symbols* while the model results are represented by the *solid lines*

run number 083 (XTC-083) was modeled. The initial concentrations of NO, NO_2, formaldehyde, acetaldehyde, *n*-octane and CO were 0.204, 0.0418, 0.0462, 0.953, 0.085 and 0.800 ppm, respectively. The temperature remained constant at 301.6 K throughout the experiment, and the NO_2 photolysis rate constant was measured as 0.256 min^{-1}. Table 4 shows how the mechanism size varied as the threshold value was reduced as well as SSE and MD values. The SSE value remained relatively constant as the threshold value was lowered while the MD value decreased with the threshold. It was also found that the number of reactions increased significantly with reductions in the threshold value. This was primarily due to the presence of a large alkane in the mixture, which has a substantial number of reaction channels available to it. Since the SSE is constant at a threshold value of 0.0001 and the MD value is below 5% at this threshold as well, this mechanism was considered to be the complete mechanism for this system.

A model of the XTC chamber using the mechanism generated with ϵ equal to 1×10^{-4} was formulated, and its predictions were compared to the experimental data. The mechanism was analyzed to determine which reactions had the most significant effect on the major species' concentrations. A subset of the mechanism that leads to formaldehyde formation is shown in Fig. 7. Specifically, small molecule reactions are

Fig. 6 The percent error in $\Delta(O_3 - NO)$ values for ETC-378, ETC-441, and ITC-1554 corresponding to formaldehyde/NO_x ratios of 0.90, 1.61, and 2.32, respectively. The percent errors are shown at 2 h intervals from 2–6 h

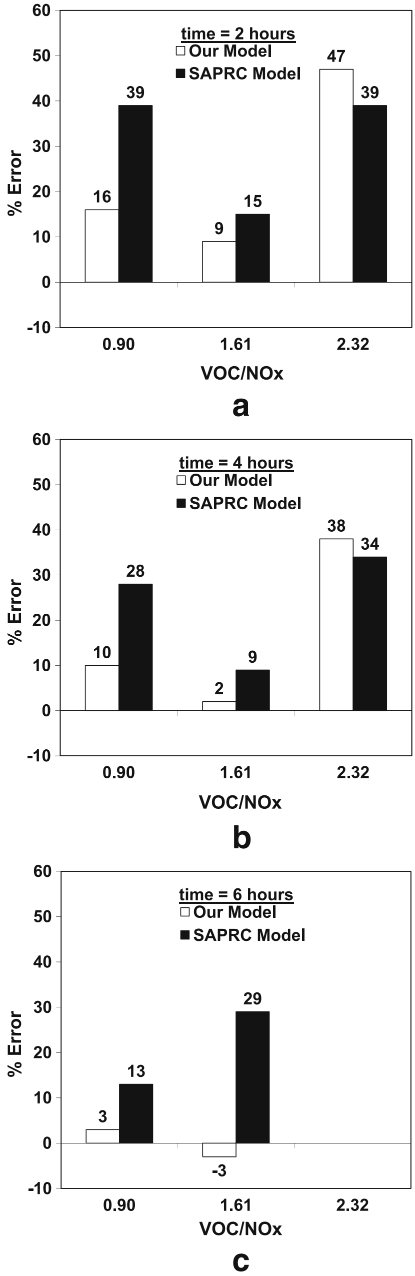

not shown and only those reactions that have net rates above 1.205×10^6 molecule cm^{-3} s^{-1} at reaction times of 2, 4, and 6 h are shown. The formaldehyde reactions illustrated in Fig. 4 are also a subset of the acetaldehyde-formaldehyde-*n*-octane-air-NO_x mechanism but are not repeated in Fig. 7. There are several pathways that lead to formaldehyde formation. These include β-scission of acetyl alkoxy radical that is

Table 4 Acetaldehyde-formaldehyde-*n*-octane-air-NO_x model as a function of mechanism generation threshold value

ε	Species	Reactions		SSE[a]	MD
		Thermal	Photolysis		
1.0	70	341	20	5.11×10^{24}	
0.1	71	345	23	5.11×10^{24}	0.00
0.01	73	353	23	5.46×10^{24}	1.91
0.001	117	702	37	6.16×10^{24}	4.01
0.0001	317	3,145	50	6.23×10^{24}	0.89

[a]SSE = sum of squares error for NO, nitrates, O_3, formaldehyde, acetaldehyde, *n*-octane, and peroxy-acetyl nitrate (PAN) and has units of molecule^2 cm^{-6}

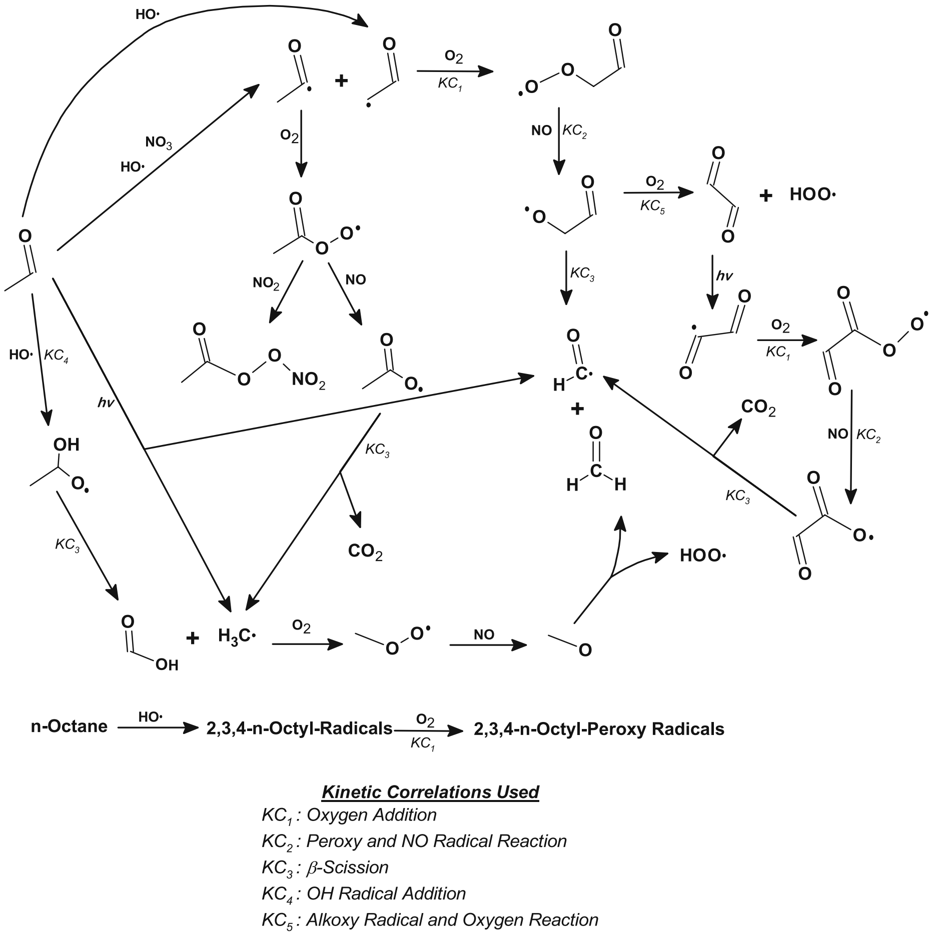

Fig. 7 The major reactions of the mechanism for reaction of a multicomponent mixture of acetaldehyde, formaldehyde, and *n*-octane generated using the conditions of XTC-083. The formaldehyde mechanism (not shown) is the same as that of Fig. 4. Reactions for the *n*-octyl radicals are not shown in detail since they are below the threshold value set. Additional detail on part of the *n*-octane decomposition pathways is provided in Fig. 8

formed from hydrogen abstraction of acetaldehyde and the reaction of methyl alkoxy radical with oxygen, the relative rates of which are approximately 2:1. The reactions of *n*-octane that lead to acetaldehyde formation from the 3- and 4-octyl radicals are shown explicitly in Fig. 8. Similar reactions that lead to acetaldehyde formation occur for the 1- and 2-octyl radicals. In the SAPRC-99 model the *n*-octane reactions are represented by Eq. 11:

$$n - Octane + OH \rightarrow RO_2\dot{R} + RO_2N + R_2\dot{O}_2 + RCHO + PROD2 + XC \quad (11)$$

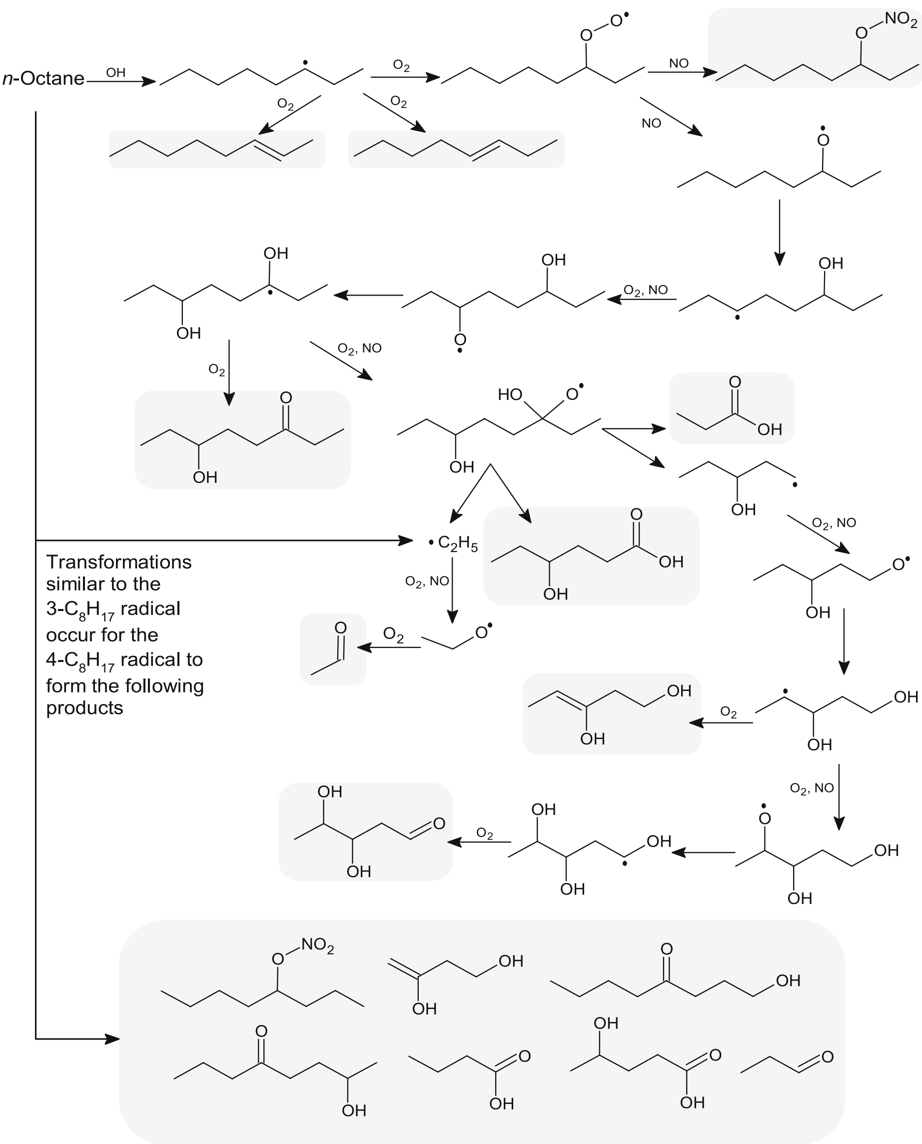

Fig. 8 The reactions that lead to acetaldehyde formation, a precursor for PAN, from *n*-octane

Each of the products in the above reaction is assigned a product yield and has its own lumped reaction. As is clear from the detailed mechanism we have developed, the reactions of *n*-octane are not as simple as the representation in Eq. 11. The model results are compared to the experimental data and the results from the SAPRC-99 model in Fig. 9. The model captures the experimental data quite well, and the agreement is comparable to that of the SAPRC-99 model.

The model generated based on the three component mixture was then applied without any parameter adjustment to two subsystems. One was the experiment of

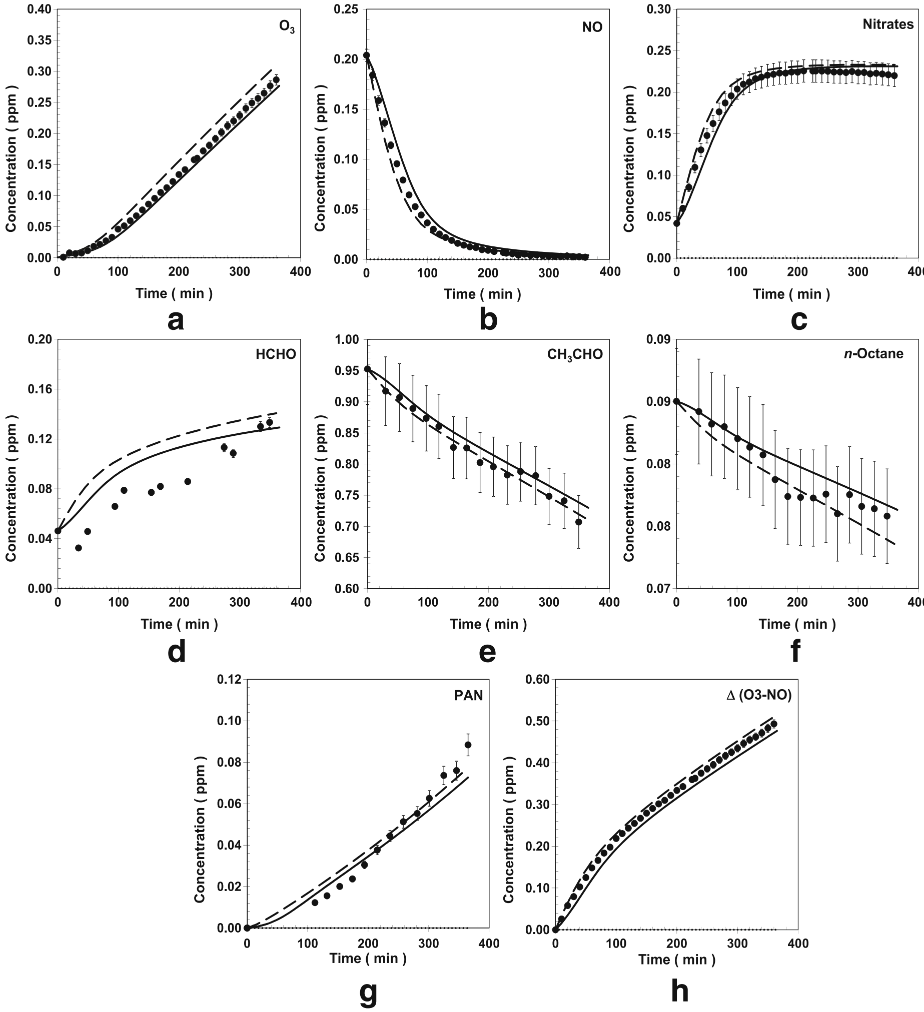

Fig. 9 Comparison of the acetaldehyde-formaldehyde-*n*-octane-air-NO_x model results to experimental data from XTC-083. The concentration versus time curves for ozone, NO, nitrates, formaldehyde, acetaldehyde, *n*-octane, PAN, and $\Delta(O_3 - NO)$ correspond to **a**–**h**, respectively. Experimental data are shown as the *symbols*, models results are shown as *solid lines* and SAPRC-99 model results are shown as *dashed lines*

acetaldehyde, *n*-octane, and NO_x conducted in a DTC chamber with run number 055b (DTC-055b), and the other was the ETC-441 experiment discussed earlier in the section on formaldehyde. These evaluations tested whether a larger mechanism generated automatically to capture a multicomponent system was applicable to smaller subsystems comprising it. The initial concentrations in the DTC-055b experiment of NO, NO_2, acetaldehyde, *n*-octane and CO were 0.0978, 0.0471, 1.25, 0.0993, and 0.800 ppm, respectively. The temperature varied linearly from 299.6 to 300.6 K, and the photolysis rate constant of NO_2 was reported as 0.388 min^{-1}. Figure 10 shows that the predicted concentrations agree well with the experimental data for the DTC-055b

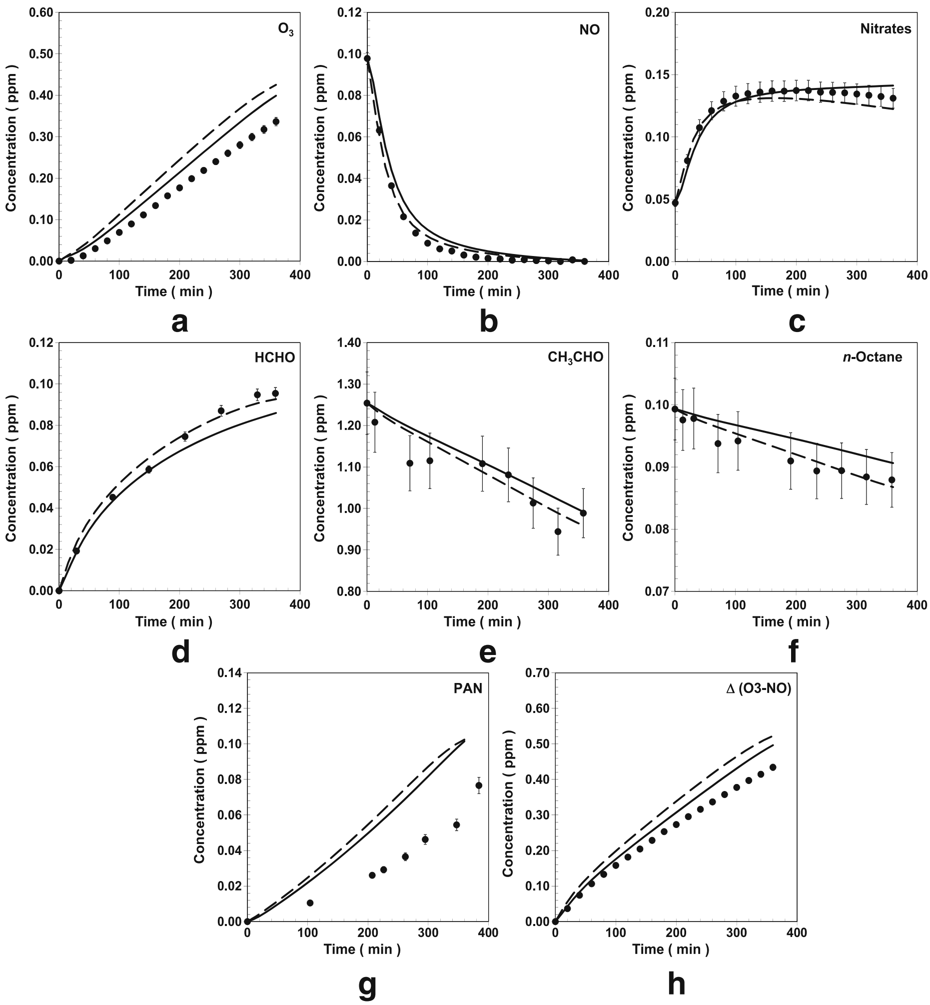

Fig. 10 Comparison of the acetaldehyde-*n*-octane model results to experimental data from DTC-055b. The concentration versus time curves for ozone, NO, nitrates, formaldehyde, acetaldehyde, *n*-octane, PAN, and $\Delta(O_3 - NO)$ correspond to **a**–**h**, respectively. Experimental data are shown as the *symbols*, models results are shown as *solid lines*, and SAPRC-99 model results are shown as *dashed lines*

smog chamber experiment. The predictions by our model were comparable to the SAPRC-99 model. The ETC-441 model results afforded a SSE value of 3.51×10^{25} molecule^2 cm^{-6} when compared to the experimental data and a MD value of 0.38 when compared to the model results presented in Fig. 3. These results were of particular note since they suggest that the methodology is sufficiently robust that one comprehensive mechanism can be generated that will apply to its constituent components.

3.3 Acetone-air-NO_x

The final system examined was acetone-air-NO_x using the rate-based methodology with the parameter set that captured the ETC-441 and XTC-083 experimental data well. SAPRC ETC chamber run number 445 (ETC-445) was used to set the initial conditions for generation and for evaluation of the model results. The initial concentrations of NO, NO_2, acetone, and CO were 0.0916, 0.0452, 8.46, and 0.800 ppm, respectively. The temperature varied linearly from 299.6 to 300.6 K, and the NO_2 photolysis rate constant was measured as 0.351 min^{-1}. The evolution of the characteristics of the mechanism as a function of the threshold value is reported in Table 5. The mechanism results changed only slightly below a threshold of 0.001 as evidenced by the values of MD below 5%. The SSE value converged to a constant value at an ϵ value of 1×10^{-5}. The mechanism at a threshold value of 0.0001 was chosen since the MD value was low and the SSE was nearly converged at that point. Initial model results revealed that the amount of ozone was over-predicted by this mechanism with the default parameters. Therefore, the mechanism was analyzed in a manner similar to that applied to probe the formaldehyde and acetaldehyde mechanisms, where reactions with net rates above 1.205×10^6 molecule cm^{-3} s^{-1} at 2, 4, and 6 h are shown in Fig. 11. Based on sensitivity analysis of the full mechanism, it was found that the mechanism was most sensitive to two reactions to an equal extent. These two reactions are listed in Eq. 12:

$$\begin{aligned} CH_3C(O)CH_2\dot{O} &\xrightarrow{O_2} CH_3C(O)C(O)H + HO\dot{O} \\ &\rightarrow CH_3\dot{C}(O) + HC(O)H \end{aligned} \tag{12}$$

The alkoxy radical and oxygen reaction was considered to be described by the less well-supported correlation of the two, and its pre-exponential factor was optimized. The rate constant for this reaction was initially estimated using the Evans–Polanyi relationship shown in Table 1 with a representative pre-exponential factor based on limited experimental data. The pre-exponential factor was optimized and was

Table 5 Acetone-air-NO_x model as a function of mechanism generation threshold value

ε	Species	Reactions		SSE[a]	MD
		Thermal	Photolysis		
1.0	28	81	14	4.79×10^{26}	
0.1	41	161	24	4.00×10^{26}	4,561.44
0.01	52	273	32	3.08×10^{26}	20.52
0.001	74	601	39	3.45×10^{26}	6.15
0.0001	148	2,577	70	3.05×10^{26}	4.10
0.00001	251	9,633	97	3.05×10^{26}	0.05
0.000001	354	22,616	125	3.05×10^{26}	0.01

[a]SSE = sum of squares error for NO, nitrates, O_3, acetone, formaldehyde, and PAN and has units of molecule^2 cm^{-6}

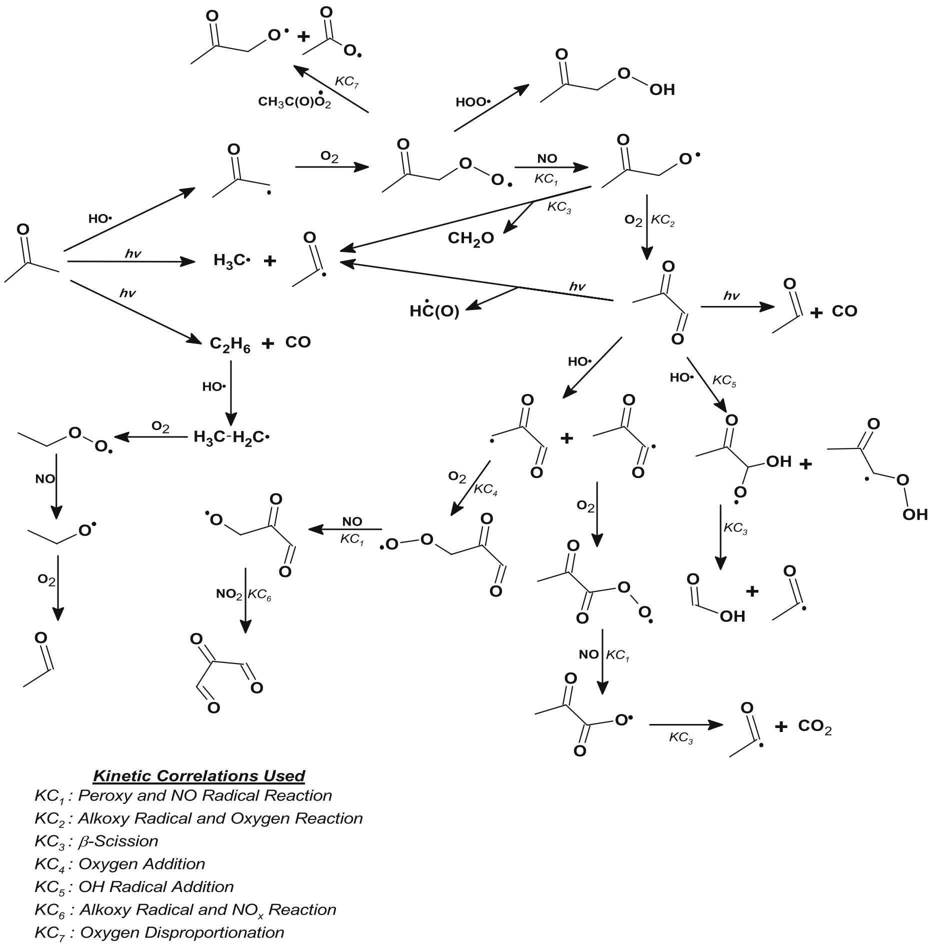

Fig. 11 The mechanism for acetone-air-NO_x with only the major reactions shown. The formaldehyde mechanism is the same as that of Fig. 4

found to be 2.00×10^{-15} cm^3 $molecule^{-1}$ s^{-1}. The optimized parameter is also listed in Table 6. Our results for this reaction agree with the findings of Orlando et al. (2000) that the decomposition of the $CH_3C(O)CH_2\dot{O}$ radical is dominated by the β-scission pathway and not the alkoxy radical and oxygen reaction pathway. A third reaction that had a major impact on the model results was the peroxy and NO radical reaction of $CH_3C(O)CH_2O\dot{O}$. The rate constant for this reaction was originally estimated using the Evans–Polanyi relationship shown in Table 1 with a representative pre-exponential factor. The pre-exponential factor was optimized and found to be 5.06×10^{-14} cm^3 $molecule^{-1}$ s^{-1}. The model results after adjustment of two pre-exponential factors (Table 6) are shown in Fig. 12, revealing that the model is able to capture the concentrations of the major species very well. Furthermore, the reactivity estimates agree very well with the experimental data. This is in contrast to the reactivity estimates from the SAPRC-99 model; our model predictions are in

Table 6 Initial and optimized values for the parameters that were optimized in the ETC-445 model for acetone-air-NO_x

Reaction	Parameter	Initial value[a]	Optimized value
$CH_3C(O)CH_2\dot{O} + O_2 \rightarrow CH_3C(O)CHO + HO\dot{O}$	A_f	2.70×10^{-14}	2.00×10^{-15}
$CH_3C(O)CH_2\dot{O} + \dot{N}O \leftrightarrow CH_3C(O)CH_2\dot{O} + \dot{N}O_2$	A_f	1.15×10^{-11}	5.06×10^{-14}

Units for all pre-exponential factors are cm^3 $molecule^{-1}$ s^{-1}

[a]Based on the representative values from part 1 of this paper

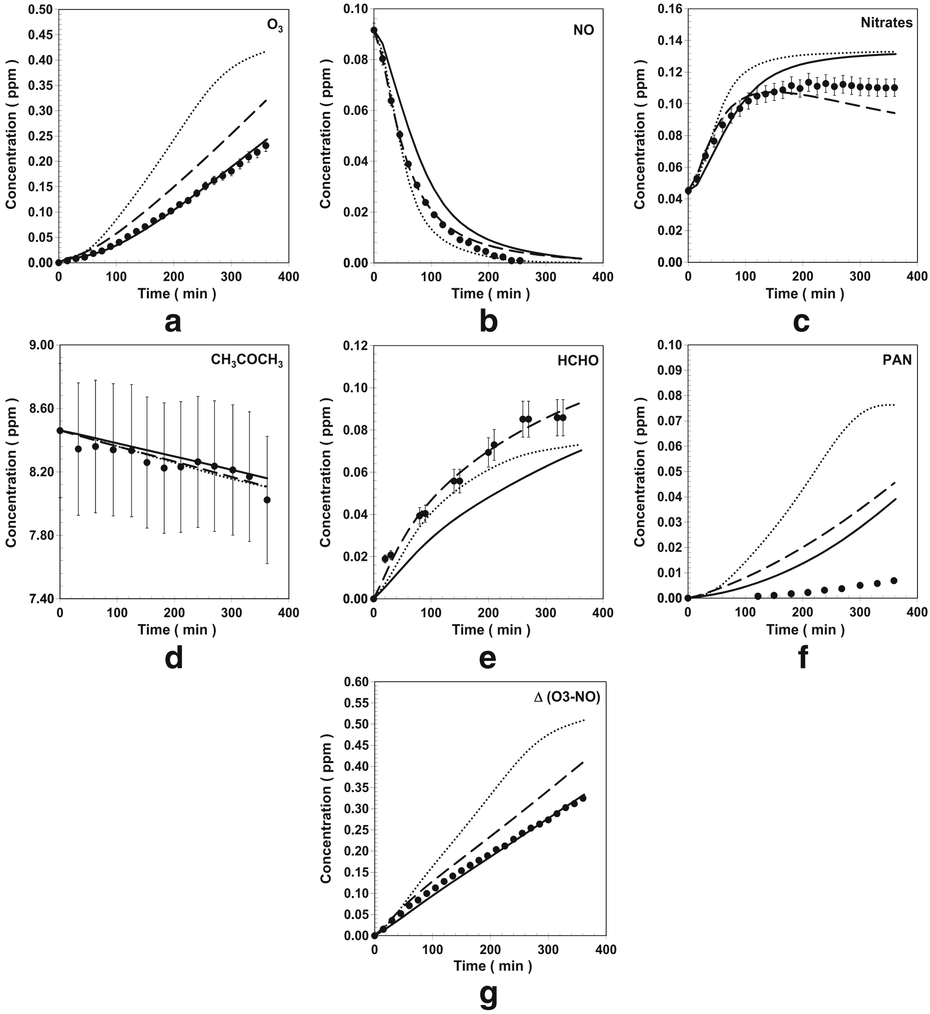

Fig. 12 Results of the acetone-air-NO_x model compared to experimental data for ETC-445. The parameters were the union of the parameters and the two parameters that were optimized specifically against the ETC-445 data. The concentration versus time curves for ozone, NO, nitrates, acetone, formaldehyde, PAN, and $\Delta(O_3 - NO)$ correspond to **a**–**g**, respectively. Experimental data are represented by *symbols*, model results before and after parameter optimization by the *dotted* and *solid lines*, respectively, and the SAPRC-99 model results by the *dashed lines*

error by −12%, −2%, and 2% while those of the SAPRC-99 mechanism are in error by 15%, 18%, and 21% at 2, 4, and 6 h, respectively.

The acetone model was then used to predict the behavior in another experiment of acetone, *n*-octane, and NO_x conducted in a DTC chamber with run number 054b (DTC-054b). The initial concentrations in the DTC-054b experiment of NO, NO_2, acetone, *n*-octane and CO were 0.1895, 0.09661, 10.97, 0.09428, and 0.800 ppm, respectively. The temperature varied linearly from 300.5 to 301.3 K, and the photolysis rate constant of NO_2 was reported as 0.388 min^{-1}. Figure 13 shows that the predicted concentrations agree well with the experimental data for the DTC-054b

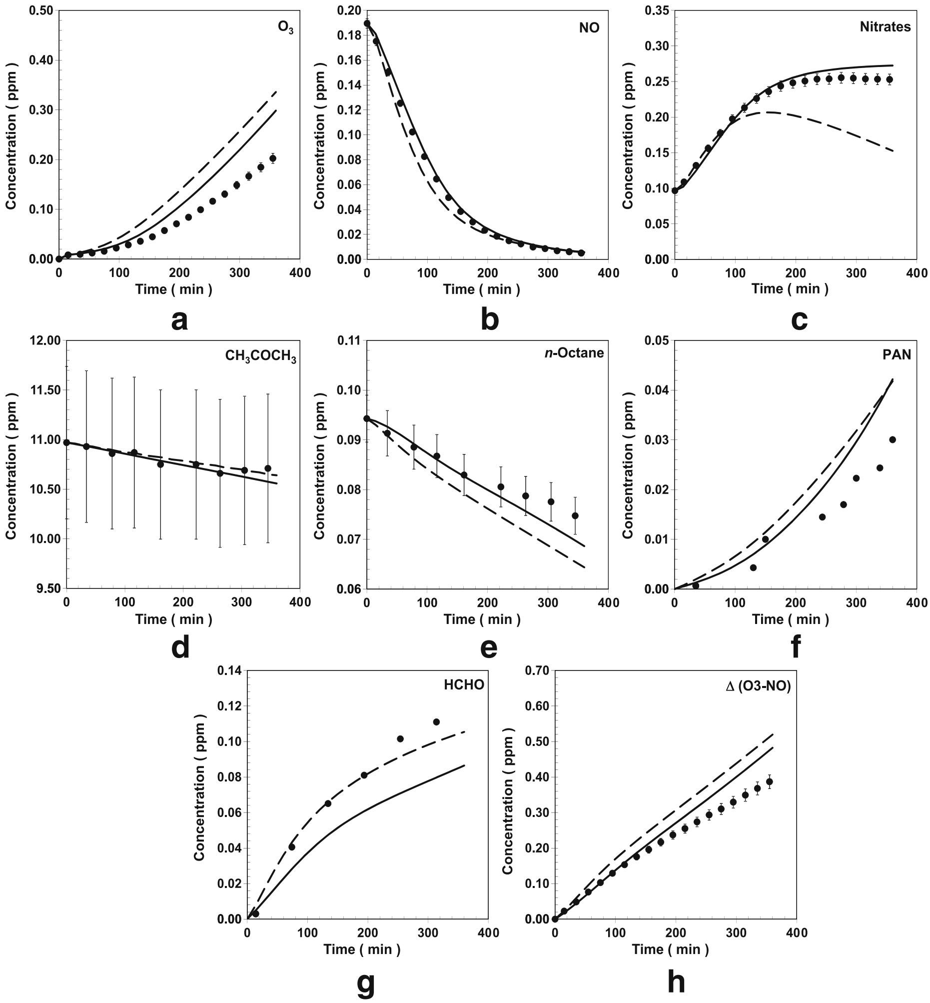

Fig. 13 Comparison of the acetone-*n*-octane model predictions to experimental data from DTC-054b. The concentration versus time curves for ozone, NO, nitrates, acetone, *n*-octane, PAN, formaldehyde and $\Delta(O_3 - NO)$ correspond to **a**–**h**, respectively. Experimental data are shown as the *symbols*, models results are shown as *solid lines*, and SAPRC-99 model results are shown as *dashed lines*

smog chamber experiment. The predictions by our model were comparable to the SAPRC-99 model. These results suggest that optimizing two representative pre-exponential factors is sufficient to describe the atmospheric chemistry of acetone well.

4 Conclusions

Mechanisms for formaldehyde-air-NO_x, acetaldehyde-formaldehyde-*n*-octane-air-NO_x, and acetone-air-NO_x were generated to model smog chamber data for UNC and SAPRC chambers. Overall, it was found that reaction mechanism growth was well controlled by using rate-based mechanism generation. For the formaldehyde-air-NO_x model, the ETC-441 experiment was used to generate the model, and this model resulted in predictions that were in reasonable agreement with experimental data from an outdoor chamber (UNC) and also data from various VOC/NO_x ratios of two other indoor chambers.

A much more complex system of acetaldehyde, formaldehyde, *n*-octane, air, and NO_x was then modeled, and without any parameter adjustments there was good agreement with experimental results for all species monitored. This model was then used to study two sub-models within it: acetaldehyde-*n*-octane-air-NO_x and formaldehyde-air-NO_x. The predictions of this large model compared well with experimental data for the two subsystems, and the results for formaldehyde-air-NO_x were the same as those for the smaller model generated for formaldehyde alone.

Finally, acetone-air-NO_x was studied. It was found that refinement of the pre-exponential factors for reaction of $CH_3C(O)CH_2\dot{O}$ alkoxy radical with oxygen to form $CH_3C(O)CHO$ and $HO\dot{O}$ and reaction of $CH_3C(O)CH_2O\dot{O}$ peroxy radical with NO to form $CH_3C(O)CH_2\dot{O}$ alkoxy radical generated model results that compared very well with experimental data. This model also performed much better than the SAPRC-99 model with respect to the reactivity estimates. Overall, the results suggest that the automated mechanism generation methodology that includes rate-based generation is sufficiently robust that it can be applied to a wide range of alkane and oxygenate mixtures.

Acknowledgement This research was funded by U.S. EPA—Science to Achieve Results (STAR) Program Grant #R-82816901-0.

References

Aschmann, S.M., Martin, P., Tuazon, E.C., Arey, J., Atkinson, R.: Kinetic and product studies of the reactions of selected glycol ethers with OH radicals. Environ. Sci. Technol. **35**(20), 4080–4088 (2001)

Atkinson, R.: Atmospheric reactions of alkoxy and β-hydroxyalkoxy radicals. Int. J. Chem. Kinet. **29**(2), 99–111 (1997)

Atkinson, R.: Atmospheric chemistry of VOCs and NO_x. Atmos. Environ. **34**(12–14), 2063–2101 (2000)

Atkinson, R., Kwok, E.S.C., Arey, J., Aschmann, S.M.: Reactions of alkoxyl radicals in the atmosphere. Faraday Discuss. **100**, 23–37 (1995)

Atkinson, R., Baulch, D.L., Cox, R.A., Hampson, R.F. Jr., Kerr, R.F., Rossi, M.J., Troe, J.: Evaluated kinetic and photochemical data for atmospheric chemistry: supplement VI—IUPAC Subcommittee on Gas Kinetic Data Evaluation for Atmospheric Chemistry. J. Phys. Chem. Ref. Data **26**(6), 1329–1499 (1997)

Atkinson, R., Tuazon, E.C., Aschmann, S.M.: Atmospheric chemistry of 2-pentanone and 2-heptanone. Environ. Sci. Technol. 34(4), 623–631 (2000)

Atkinson, R., Baulch, D.L., Cox, R.A., Crowley, J.N., Hampson, R.F. Jr., Kerr, J.A., Rossi, M.J., Troe, J.: Summary of Evaluated Kinetic and Photochemical Data for Atmospheric Chemistry IUPAC Subcommittee on Gas Kinetic Data Evaluation for Atmospheric Chemistry. Working Paper (2001)

Atkinson, R., Baulch, D.L., Cox, R.A., Crowley, J.N., Hampson, R.F. Jr., Hynes, R.G., Jenkin, M.E., Rossi, M.J., Troe, J.: Evaluated kinetic and photochemical data for atmospheric chemistry: volume I—gas phase reactions of O_x, HO_x, NO_x and SO_x species. Atmos. Chem. Phys. **4**, 1461–1738 (2004)

Aumont, B., Szopa, S., Madronich, S.: Modelling the evolution of organic carbon during its gas-phase tropospheric oxidation: Development of an explicit model based on a self generating approach. Atmos. Chem. Phys. **5**, 2497–2517 (2005)

Becker, E., Rahman, M.M., Schindler, R.N.: Determination of the rate constants for the gas phase reactions of NO_3 with H, OH and HO_2 radicals at 298 K. Ber. Bunsenges. Phys. Chem. **96**, 776–783 (1992)

Blowers, P., Masel, R.I.: An extension of the Marcus equation for atom transfer reactions. J. Phys. Chem. A. **103**(35), 7047–7054 (1999)

Bowman, F.M., Seinfeld, J.H.: Fundamental basis of incremental reactivities of organics in ozone formation in VOC/NO_x mixtures. Atmos. Environ. **28**(20), 3359–3368 (1994)

Broadbelt, L.J., Stark, S.M., Klein, M.T.: Computer generated pyrolysis modeling: on-the-fly generation of species, reactions, and rates. Ind. Eng. Chem. Res. **33**(4), 790–799 (1994a)

Broadbelt, L.J., Stark, S.M., Klein, M.T.: Computer generated reaction networks: on-the-fly calculation of species properties using computational quantum chemistry. Chem. Eng. Sci. **49**(24B), 4991–5010 (1994b)

Broadbelt, L.J., Stark, S.M., Klein, M.T.: Termination of computer-generated reaction mechanisms: species rank-based convergence criterion. Ind. Eng. Chem. Res. **34**(8), 2566–2573 (1995)

Broadbelt, L.J., Stark, S.M., Klein, M.T.: Computer generated reaction modelling: decomposition and encoding algorithms for determining species uniqueness. Comput. Chem. Eng. **20**(2), 113–129 (1996)

Calvert, J.G., Atkinson, R., Kerr, J.A., Madronich, S., Moortgat, G.K., Wallington, T.J., Yarwood, G.: The Mechanisms of Atmospheric Oxidation of the Alkenes. Oxford University Press, New York (2000)

Carter, W.P.L.: Development of ozone reactivity scales for volatile organic compounds. J. Air Waste Manage. Assoc. **44**(7), 881–899 (1994)

Carter, W.P.L.: Documentation of the SAPRC-99 Chemical Mechanism for VOC Reactivity Assessment. Working Paper, University of California, Riverside, California, Final Report to California Air Resources Board (2000)

Carter, W.P.L., Atkinson, R.: An experimental study of incremental hydrocarbon reactivity. Environ. Sci. Technol. **21**(7), 670–679 (1987)

Carter, W.P.L., Atkinson, R.: Computer modeling study of incremental hydrocarbon reactivity. Environ. Sci. Technol. **23**(7), 864–880 (1989)

Carter, W.P.L., Atkinson, R.: Development and evaluation of a detailed mechanism for the atmospheric reactions of isoprene and NO_x. Int. J. Chem. Kinet. **28**(7), 497–530 (1996)

Carter, W.P.L., Lurmann, F.W.: Evaluation of a detailed gas-phase atmospheric reaction mechanism using environmental chamber data. Atmos. Environ. **25A**(12), 2771–2806 (1991)

Carter, W.P.L., Dongmin, L., Malkina, I.L., Fitz, D.: The University of California, Riverside Environmental Chamber Data Base for Evaluating Oxidant Mechanisms. Working Paper, University of California, Riverside, California, Report to US-EPA (1993)

Carter, W.P.L., Luo, D., Malkina, I.L., Pierce, J.A.: Environmental Chamber Studies of Atmospheric Reactivities of Volatile Organic Compounds. Effects of Varying Chamber and Light Source. Working Paper, University of California, Riverside, California, Final Report to National Renewable Energy Laboratory, Coordinating Research Council, Inc., California Air Resources Board, and South Coast Air Quality Management District (1995)

De Witt, M.J.: Elucidation of the Primary Reaction Pathways and Degradation Mechanism during Coprocessing of Polymeric Waste with Coal. Ph.D. Thesis, Northwestern University, Evanston, IL (1999)

DeMore, W.B., Sander, S.P., Golden, D.M., Hampson, R.F. Jr., Kurylo, M.J., Howard, C.J., Ravishankara, A.R., Kolb, C.E., Molina, M.J.: Chemical Kinetics and Photochemical Data for Use in Stratospheric Modeling, Evaluation No. 12. Working Paper, Jet Propulsion Laboratory, Pasadena, CA (1997)

Derwent, R.G., Jenkin, M.E., Saunders, S.M.: Photochemical ozone creation potentials for a large number of reactive hydrocarbons under European conditions. Atmos. Environ. **30**(2), 181–199 (1996)

DeWitt, M.J., Dooling, D.J., Broadbelt, L.J.: Computer generation of reaction mechanisms using quantitative rate information: application to long-chain hydrocarbon pyrolysis. Ind. Eng. Chem. Res. (7), 2228–2237 (2000)

Dodge, M.C.: Chemical oxidant mechanisms for air quality modeling: critical review. Atmos. Environ. **34**(12–14), 2103–2130 (2000)

Dunlea, E.J., Ravishankara, A.R.: Measurement of the rate coefficient for the reaction of $O(^1D)$ with H_2O and re-evaluation of the atmospheric OH production rate. Phys. Chem. Chem. Phys. **6**, 3333–3340 (2004)

Evans, M.G., Polanyi, M.: Inertia and driving force of chemical reactions. T. Faraday Soc. **34**, 11–29 (1938)

Finlayson-Pitts, B.J., Pitts, J.N. Jr.: Chemistry of the Upper and Lower Atmosphere: Theory, Experiments, and Applications. Academic, San Diego (1999)

Gery, M.W., Whitten, G.Z., Killus, J.P., Dodge, M.C.: A photochemical kinetic mechanism for urban and regional scale computer modeling. J. Geophys. Res. **94**(D10), 12925–12956 (1989)

Hillewaert, L.P., Dierickx, J.L., Froment, G.F.: Computer generation of reaction schemes and rate equations for thermal cracking. AIChE J. **34**(1), 17–24 (1988)

Jeffries, H.E., Sexton, K.G., Kamens, R.M., Holleman, M.S.: Outdoor Smog Chamber Experiments to Test Photochemical Models: Phase II. Working paper EPA/600/3-85/029, Report to the U.S. Environmental Protection Agency (1985)

Jenkin, M.E., Saunders, S.M., Pilling, M.J.: The tropospheric degradation of volatile organic compounds: a protocol for mechanism development. Atmos. Environ. **31**(1), 81–104 (1997)

Johnston, H.S., Davis, H.F., Lee, Y.T.: NO_3 photolysis product channels: quantum yields from observed energy thresholds. J. Phys. Chem. **100**(12), 4713–4723 (1996)

Kanno, N., Tonokura, K., Koshi, M.: Equilibrium constant of the HO_2-H_2O complex formation and kinetics of $HO_2 + HO_2$-H_2O: implications for tropospheric chemistry. J. Geophys. Res. **111**, 20312 (2006)

Khan, S.S., Broadbelt, L.J.: A group additivity approach for the prediction of wavelength-dependent absorption cross-sections. Atmos. Environ. **38**(7), 1015–1022 (2004)

Kirchner, F., Stockwell, W.R.: Effect of peroxy radical reactions on the predicted concentrations of ozone, nitrogenous compounds, and radicals. J. Geophys. Res. **101**(D15), 21007–21022 (1996)

Madronich, S., Calvert, J.G.: Permutation reactions of organic peroxy radicals in the troposphere. J. Geophys. Res. **95**(D5), 5697–5715 (1990)

Makar, P.A., Polavarapu, S.M.: Analytic solutions for gas-phase chemical mechanism compression. Atmos. Environ. **31**(7), 1025–1039 (1997)

Makar, P.A., Stockwell, W.R., Li, S.M.: Gas-phase chemical mechanism compression strategies: treatment of reactants. Atmos. Environ. **30**(6), 831–842 (1996)

Matheu, D.M., Lada, T.A. II, Green, W.H., Dean, A.M., Grenda, J.M.: Rate-based screening of pressure-dependent reaction networks. Comput. Phys. Commun. **138**(3), 237–249 (2001)

Molina, L.T., Molina, M.J.: Absolute absorption cross sections of ozone in the 185- to 350-nm wavelength range. J. Geophys. Res. **91**, 14501–14508 (1986)

Orlando, J.J., Tyndall, G.S., Vereecken, L., Peeters, J.: The atmospheric chemistry of the acetonoxy radical. J. Phys. Chem. A **104**(49), 11578–11588 (2000)

Pfaendtner, J., Broadbelt, L.J.: Mechanistic modeling of lubricant degradation. Part 1: structure–reactivity relationships for free-radical oxidation. Ind. Eng. Chem. Res. **47**(9), 2886–2896 (2008a)

Pfaendtner, J., Broadbelt, L.J.: Mechanistic modeling of lubricant degradation. Part 2: the autoxidation of decane and octane. Ind. Eng. Chem. Res. **47**(9), 2897–2904 (2008b)

Ranzi, E., Gaffuri, P., Faravelli, T., Dagaut, P.: A wide-range modeling study of n-heptane oxidation. Combust. Flame. **103**(1–2), 91–106 (1995)

Saunders, S.M., Pascoe, S., Johnson, A.P., Pilling, M.J., Jenkin, M.E.: Development and preliminary test results of an expert system for the automatic generation of tropospheric VOC degradation mechanisms. Atmos. Environ. **37**(13), 1723–1735 (2003)

Stockwell, W.R., Middleton, P., Chang, J.S. Tang, X.: The second generation regional acid deposition model chemical mechanism for regional air quality modeling. J. Geophys. Res. **95**, 16343–16367 (1990)

Stockwell, W.R., Kirchner, F., Kuhn, M., Seefeld, S.: A new mechanism for regional atmospheric chemistry modeling. J. Geophys. Res. **102**, 25847–25880 (1997)

Susnow, R.G., Dean, A.M., Green, W.H. Jr., Peczak, P., Broadbelt, L.J.: Rate-based construction of kinetic models for complex systems. J. Phys. Chem. A **101**(20), 3731–3740 (1997)

Talukdar, R.K., Longfellow, C.A., Gilles, M.K., Ravishankara, A.R.: Quantum yields of $O(^1D)$ in the photolysis of ozone between 289 and 329 nm as a function of temperature. Geophys. Res. Lett. **25**(2), 143–146 (1998)

Tarjan, R.E.: Graph Algorithms in Chemical Computation. Algorithms for Chemical Computations. American Chemical Society, Washington, DC (1977)

Tomlin, A.S., Pilling, M.J., Turányi, T., Merkin, J.H., Brindley, J.: Mechanism reduction for the oscillatory oxidation of hydrogen sensitivity and quasi-steady state analyses. Combust. Flame. **91**, 107–130 (1992)

Ugi, I., Bauer, J., Brandt, J., Friedrich, J., Gasteiger, J., Jochum, C., Schubert, W.: New applications of computers in chemistry. Angew. Chem. Int. Edit. Engl. **18**(2), 111–123 (1979)

Wong, H.-W., Li, X.G., Swihart, M.T., Broadbelt, L.J.: Detailed kinetic modeling of silicon nanoparticle formation chemistry via automated mechanism generation. J. Phys. Chem. A **108**(46), 10122–10132 (2004a)

Wong, H.-W., Nieto, J.C.A., Swihart, M.T., Broadbelt, L.J.: Thermochemistry of silicon-hydrogen compounds generalized from quantum chemical calculations. J. Phys. Chem. A **108**(5), 874–897 (2004b)